Sonolytic Destruction of Methyl tert Butyl Ether by Ultrasonic Irradiation: The Role of O 3 , H 2 O 2 , Frequency, and Power Density

ARTICLE *in* ENVIRONMENTAL SCIENCE AND TECHNOLOGY · SEPTEMBER 1999

Impact Factor: 5.33 · DOI: 10.1021/es9810383

Environ. Sci. Technol. **1999**, *33,* 3199−3205

Sonolytic Destruction of Methyl *tert*-Butyl Ether by Ultrasonic Irradiation: The Role of O_3, H_2O_2, Frequency, and Power Density

JOON-WUN KANG,† HUI-MING HUNG, ANGELA LIN, AND MICHAEL R. HOFFMANN*

W. M. Keck Laboratories, California Institute of Technology, Pasadena, California 91125

The kinetics of degradation of methyl *tert*-butyl ether (MTBE) by ultrasonic irradiation in the presence of ozone as functions of applied frequencies and applied power are investigated. Experiments are performed over the frequency range of 205−1078 kHz. The higher overall reaction rates are observed at 358 and 618 kHz and then at 205 and 1078 kHz. The observed pseudo-first-order rate constant, k_0, for MTBE degradation increases with increasing power density up to 250 W L^{-1}. A linear dependence of the first-order rate constant, k_{O_3}, for the simultaneous degradation of O_3 on power density is also observed. Naturally occurring organic matter (NOM) is shown to have a negligible effect on observed reaction rates.

Introduction

Methyl *tert*-butyl ether (MTBE) which is blended into gasoline, is frequently found in groundwater, where it is slowly degraded by aerobic and anaerobic processes (*1*).

The application of ultrasound for the treatment of chemical contaminants in water has been explored in recent years (*2*−*8*). Ultrasonic waves, which consist of compression and rarefaction cycles, produce cavitation bubbles in liquid solution. After several compression cycles, the cavitation bubbles collapse violently and adiabatically with extremely high temperatures up to 5000 K and pressures of 975 bar (*9*,*10*). Under these extreme conditions, volatile chemical compounds are destroyed by direct pyrolysis reactions and indirectly by reactions with H•, •OH, O•, and H_2O_2. The addition of ozone into sonolytic systems often enhances the overall rate of destruction of a wide variety of compounds (*6*,*11*,*12*).

The thermal decomposition of ozone in cavitation bubbles leads to the formation of •OH as shown in eqs 1 and 2 (*11*,*13*). In addition, the direct reaction of ozone with substrates may occur.

$$O_3 \rightarrow O_2 + O(^3P) \quad (1)$$

$$O(^3P) + H_2O \rightarrow {}^{2\bullet}OH \quad (2)$$

In our preceding paper (*14*), the kinetics and mechanism of sonolytic degradation of MTBE were investigated at a single ultrasonic frequency of 205 kHz. The addition of ozone into the aqueous sonolytic system resulted in an increased rate of MTBE destruction. The generalized reactions can be described by the following equations.

$$(CH_3)_3COCH_3 \xrightarrow{))),\ H_2O} (CH_3)_3COH + CH_3OH \quad (3)$$

$$(CH_3)_3COCH_3 \xrightarrow{))),\ O_3,\ H_2O} (CH_3)_3COH + HCO_2H \quad (4)$$

$$(CH_3)_3COH \xrightarrow{))),\ H_2O} (CH_3)_3CO_2H,\ CH_3OH,\ HCHO \quad (5)$$

$$(CH_3)_3COCH_3 \xrightarrow{))),\ O_3} (CH_3)_3COOCH_3 \xrightarrow{)))} CH_3OH,\ HCO_2H \quad (6)$$

where the symbol))) indicates ultrasonic irradiation. The main intermediates observed during MTBE sonolysis and ozonolysis are *tert*-butyl formate and *tert*-butyl alcohol. In this paper, the combined effects of sonolysis and ozonolysis on the kinetics of MTBE degradation are explored over a broader frequency range.

Experimental Methods

MTBE (99.9%; EM science) and sodium bicarbonate (Reagent Grade; EM Science) were used without further purification. A humic acid reagent was prepared by dissolving solid humic acid obtained from Fluka AG in a 0.1 N NaOH solution and then filtering through 0.45 μm filter paper.

Ultrasonic irradiations were performed with an Ultrasonic Transducer USW 51 (AlliedSignal ELAC Nautik, Inc.) in a glass and titanium reactor, which has a vibrational surface area of 25 cm^2 and can be operated at four different frequencies: 205, 358, 618, and 1078 kHz. The reaction volume, as shown in Figure 1, is contained within a 600 mL cylindrical, double-walled (i.e., water-cooled) reaction vessel, that has four sampling ports on the top which are used for gas venting, for withdrawing aqueous samples, and for the introduction of background gases.

Temperature was maintained constant at 23 ± 3 °C with a 20 °C refrigerated water bath (Haake Co., model A80). Aqueous solutions were made with water obtained from a MilliQ UV + purification system. Ozone solutions were prepared with an Orec Ozonator (model V10-0) by bubbling ozone into deionized water at a flow rate of 100 mL min^{-1} through a glass fritted diffuser until the desired ozone concentration in the aqueous phase was obtained. Ozone concentrations were obtained spectrophotometrically using a HP 8452 diode array spectrophotometer; the molar extinction coefficient for O_3 in water at 260 nm is 3300 M^{-1} cm^{-1}.

MTBE stock solutions (100 mM) were prepared and stored at 4 °C. After the desired aqueous ozone concentration was obtained, an appropriate volume of the MTBE stock solution was spiked into 500 mL of ozonated solution to initiate the sonochemical reaction. Additional mixing was achieved by bubbling O_2/O_3 gas for a few more seconds at a low flow rate in order to minimize any sparging effects. The first sample was taken immediately after closing off the ozone supply. After the $t = 0$ sample was taken, ultrasonic irradiation was initiated. Sample aliquots (i.e., 1.0 mL) were taken at appropriate time intervals during each kinetic run and stored in 20 mL Teflon-capped, aluminum-sealed vials. In the case of dissolved ozone, 10 μL of 1 N $Na_2S_2O_3$ was used to quench

* To whom correspondence should be addressed. Phone: (626) 395-4391; fax: (626) 395-3170; e-mail: mrh@cco.caltech.edu.

† Current address: Department of Industrial Environment and Health, Yonsei University Wonju Campus, 234 Maeji, Wonju, KOREA (220-710).

10.1021/es9810383 CCC: $18.00
Published on Web 08/04/1999

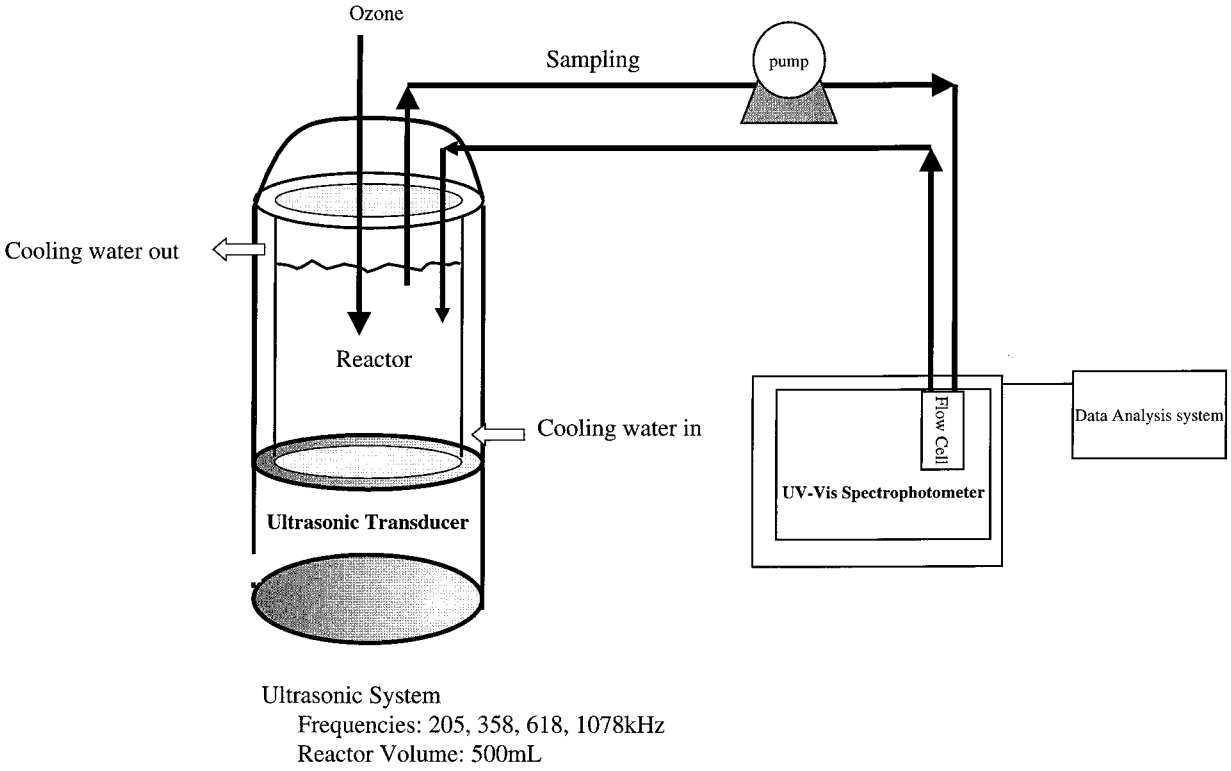

FIGURE 1. Schematic diagram of the sonochemical−reactor system.

the residual aqueous ozone to preserve samples prior to the analysis. Since the total amount of samples withdrawn from the reactor was kept to less than 15 mL, only a small error (<3%) was introduced due to the differential volume change. During each kinetic run, the ultrasonic power inputs were kept in the range of 50−240 W, depending on the particular ultrasonic frequency that was used. For frequencies greater than 600 kHz, the maximum applied power was 50 W.

Compounds extracted into the gas phase of the HP 7694 headspace sampler were autoinjected into a HP 5890 series II GC-FID equipped with a HP-624 capillary column (30 m × 0.32 mm × 1.8 um) with a 70 °C isothermal oven temperature. Sample aliquots for hydrogen peroxide analysis were taken at 10 min intervals and were measured by spectrofluorometer (*9*). Samples taken for TOC (total organic carbon) analysis were filtered with 0.45 μm Teflon syringe filters (Gelman) before injection and were measured with a Shimadzu 5000A total organic carbon analyzer.

For some runs, the aqueous ozone concentrations were continuously measured spetrophotometrically with circulation of the aqueous solution from the reactor through the spectrophotometer and back into the reactor.

Results and Discussion

Effects of Applied Power Input. In our earlier study, which was carried out at 205 kHz, the sonolytic degradation of MTBE was shown to follow pseudo-first-order kinetics. Plots of the pseudo-first-order rate constants, k_0, versus the input power density are shown in Figure 2 for sonolytic irradiation at 205 and 358 kHz with initial MTBE concentrations of 1 and 0.05 mM, respectively. The apparent rate constant, $k_{0,358}$, at 358 kHz is higher than $k_{0,205}$ by a factor of 5. From our previous study (*14*), the MTBE sonication rate constant at 205 kHz was found to be faster with $[MTBE]_0 = 0.05$ mM than for $[MTBE]_0 = 1$ mM by a factor of 2 (i.e., the rate decreases with increase initial substrate concentration). Furthermore, as shown in Figure 2, k_0 increases rapidly with an increase in power density up to 240 W L^{-1}. In general, an increase in power density results in an increase in the observed

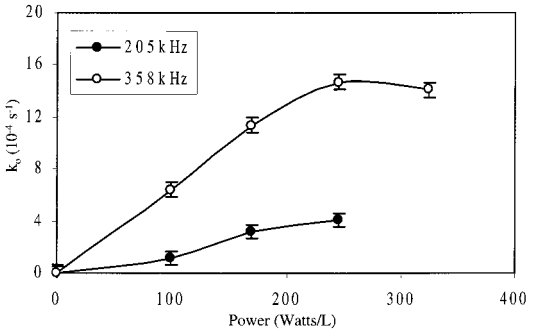

FIGURE 2. Effect of power density on the pseudo-first-order rate constant, k_0, for the destruction of MTBE by ultrasonic irradiation at 205 and 358 kHz: $[MTBE]_0 = 1$ mM at 205 kHz; $[MTBE]_0 = 0.05$ mM at 358 kHz.

sonochemical reaction rate. However, the cavitation bubble size, the bubble collapse time, the transient temperature, and the internal pressure in the cavitation bubble during collapse are all dependent on the power intensity. For example, the power intensity, which is proportional to the applied power density, is a function of the acoustic amplitude, P_A as follows:

$$I = P_A^2/2\rho c \tag{7}$$

where I is the sound intensity (amount of energy flowing per unit area per unit time), ρ is the density of the medium, and c is the velocity of sound in the medium.

For a cavitation bubble, the maximum bubble size is dependent on the density of the liquid, the applied frequency, the hydrostatic pressure, and the acoustic pressure as follows (*9*):

$$R_{max} = \frac{4}{3\omega_a}(P_A - P_h)\left(\frac{2}{\rho P_A}\right)^{1/2}\left[1 + \frac{2}{3P_h}(P_A - P_h)\right]^{1/3} \tag{8}$$

where ω_a is the applied acoustic frequency and P_h is the external (hydrostatic) pressure, which is 1 atm under our experimental conditions. In addition, the bubble collapse time, τ, is proportional to the maximum bubble size, R_m (*9*):

$$\tau = 0.915R_m(\rho/P_m)^{1/2}(1 + P_{vg}/P_m) \quad (9)$$

where P_m is the pressure in the liquid (i.e., $P_m = P_h + P_a$) and P_{vg} is the vapor pressure in the bubble. Therefore, at high acoustic intensity (i.e., large P_A values) the cavitation bubbles are able to grow larger in size during a rarefaction cycle such that insufficient time is available for complete collapse during a single compression cycle. As the above equations predict and the experimental results show, there is an optimum power density which can be applied during sonochemical irradiation in order to obtain maximum reaction rates.

Effects of Variable Frequencies on H_2O_2 Production. In an attempt to determine the optimum frequency to obtain the most beneficial chemical effects, hydrogen peroxide production was used as a direct indicator of free radical production. Hydrogen peroxide is produced during the sonolysis of water (*5*,*9*,*13*). During sonolysis, hydrogen atoms and hydroxyl radicals are formed due to the pyrolytic decomposition of water.

$$H_2O \rightarrow H^\bullet + {}^\bullet OH \quad (10)$$

Hydroxyl radicals can recombine to form hydrogen peroxide:

$${}^\bullet OH + {}^\bullet OH \rightarrow H_2O_2 \quad (11)$$

If O_2 is present in the vapor phase of the bubble, peroxide can also be produced via the production of the hydroperoxyl radical as follows:

$$H^\bullet + O_2 \rightarrow HO_2^\bullet \quad (12)$$

$$HO_2^\bullet + HO_2^\bullet \rightarrow H_2O_2 + O_2 \quad (13)$$

Since the self-reaction rate constants of $HO_2^\bullet$ and ${}^\bullet OH$ at 298 K are 8.3×10^5 and 5.5×10^9 M^{-1} s^{-1} in solution (*15*) and 3×10^{-12} (*16*) and 1.5×10^{-11} cm^3 $molecule^{-1}$ s^{-1} (*17*) in the gas phase, respectively, the ${}^\bullet OH$ recombination reaction should be the major route for the hydrogen peroxide formation. The sonolytic production rates of H_2O_2 in O_2-saturated solutions relative to Ar-saturated solutions were compared at 205 kHz with a power density of 240 W/L. The apparent H_2O_2 production rates for these two conditions were found to be identical; i.e., $d[H_2O_2]/dt = 3.5 \times 10^{-4}$ mM min^{-1}. This result supports the argument that the self-reaction (eq 11) of OH is the principal pathway for H_2O_2 production.

Recombination of $OH^\bullet$ to form H_2O_2 most likely takes place in the bubble phase instead of the liquid phase (*18*). It should also noted that hydrogen peroxide is the most likely $OH^\bullet$ scavenger ($k_{OH,H_2O_2} = 2.7 \times 10^7$ M^{-1} s^{-1}) in the absence of other $OH^\bullet$ scavengers (*19*).

$$OH^\bullet + H_2O_2 \rightarrow HO_2^\bullet + H_2O \quad (14)$$

The rate of hydrogen peroxide production during the sonolysis of water is given by eq 15. The actual production rates of ${}^\bullet OH$ and H_2O_2 during sonolysis will be affected by the bubble collapse temperature, the collapse pressure, and the bubble lifetime.

$$d[H_2O_2]/dt = k_{OH,OH}[OH][OH] + k_{HO_2,HO_2}[HO_2][HO_2] - k_{OH,H_2O_2}[OH][H_2O_2] - k_{pyr}[H_2O_2] \quad (15)$$

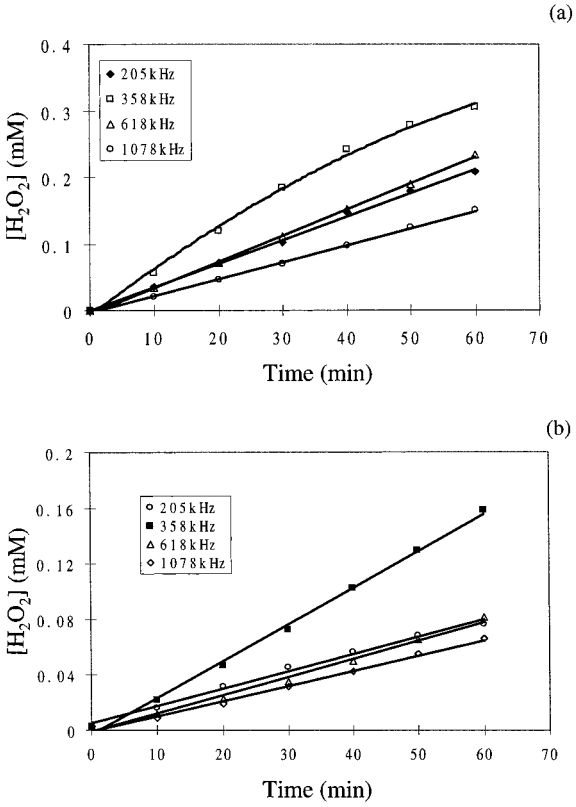

FIGURE 3. (a) Effect of frequency on hydrogen peroxide production rate at power density = 240 W/L. (b) Effect of frequency on hydrogen peroxide production rate at power density = 100 W/L.

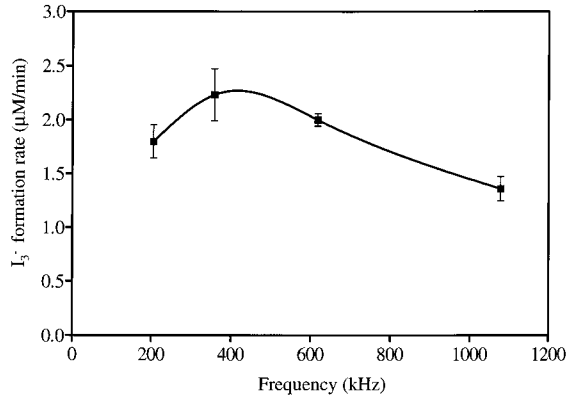

FIGURE 4. I_3^- production rate at 205, 358, 618, and 1078 kHz with $[KI]_0 = 0.1$ M, temperature 23 ± 3 °C, and power density 84 W L^{-1}.

Plots of hydrogen peroxide (H_2O_2) production versus time with a power input of 240 W/L are shown in Figure 3a for four different sonolytic frequencies: 205, 358, 618, and 1078 kHz. At a power input of 100 W L^{-1}, a similar trend with a variation in frequency is observed in Figure 3b. However, in this case the rates of H_2O_2 production are lower due to the lower applied power density (i.e., lower P_A). The peroxide production rate, $d[H_2O_2]/dt$, at 240 W L^{-1} is approximately twice that at 100 W L^{-1} and is clearly highest at 358 kHz and lowest at 1078 kHz. From the data shown in Figure 3a, it is worthwhile to note that peroxide production at 358 kHz is nonlinear, whereas for the other frequency. This may be due to the fact that the self-scavenging reaction between OH radical and H_2O_2 (eq 14) becomes significant as peroxide accumulates in the liquid phase. Hua and Hoffmann (*5*) reported that $d[H_2O_2]/dt$ increased with increasing frequency for 20, 40, 80, and 500 kHz. However, it is noted that the peroxide production rate is the lowest at the highest applied

TABLE 1. Enhancement Effect of Ozone on the Pseudo-First-Order Rate Constants of MTBE Destruction

	k_0, 10^{-4} s^{-1} at 205 kHz				k_0, 10^{-4} s^{-1} at 358 kHz					
									R^c	
[MTBE], mM	O_3, mM	US[a]	O_3–US	E^b	O_3, mM	US	O_3–US	E^b	US	O_3–US
0.01	0.30	8.5	33.2	3.9	0.20	16.5	88.3	5.4	1.9	2.7
0.25	0.31	6.9	14.9	2.2	0.23	15.3	32.2	2.1	2.2	2.1
0.50	0.34	5.4	12.2	2.3	0.23	10.4	18.6	1.8	1.9	1.5
1.00	0.26	4.1	6.3	1.5	0.23	6.8	12.3	1.8	1.7	2.0

[a] US = ultrasound. [b] Enhancement factor = k_0(O_3–ultrasound)/k_0(ultrasound). [c] Ratio = k_0(358kHz)/k_0(205kHz).

ultrasonic frequency of 1078 kHz. At these very high frequencies, the rarefaction (and compression) cycles are very short. The time required for the rarefaction cycle is too short to permit a cavitation bubble to grow to a size sufficient to cause optimal disruption of the liquid.

The I_2 (I_3^-) production rate during sonolysis at four different frequencies is shown in Figure 4. The iodine formation rate can be related to the $^\bullet$OH production rate by a stoichiometric factor of 2. The sequence of I^- oxidation is as follows:

$$^\bullet OH + I^- \rightarrow OH^- + I^\bullet \quad (16)$$

$$I^\bullet + I^- \rightarrow I_2^{\bullet -} \quad (17)$$

$$I_2^{\bullet -} + I^\bullet \rightarrow I_3^- \quad (18)$$

$$I_2^{\bullet -} + OH^\bullet \rightarrow I_2 + OH^- \quad (19)$$

$$I_2 + I^- \rightleftharpoons I_3^- \quad (20)$$

Again, the optimum frequency for I_2 (I_3^-) production at 293 K and $I_a = 84$ W L^{-1} is located between 358 and 618 kHz. This result is similar to that observed for H_2O_2 production although the reaction volume for H_2O_2 can be with the vapor phase of the collapsing bubble or within the interfacial region of the bubble, whereas I_3^- formation is restricted to the liquid phase (*20*).

Enhancement Effects of O_3 on MTBE Degradation at 205 and 358 kHz. The combination of O_3 and ultrasound at 205 kHz has been shown to enhance the MTBE degradation rate (*14*). In this study, the enhancement effect of O_3 in sonolytic MTBE degradation at 358 kHz was investigated and compared with the 205 kHz data (Table 1). The direct reaction of MTBE with ozone has a pseudo-first-order constant of 6×10^{-5} s^{-1} for $[MTBE]_0 = 0.01$ mM and 6.7×10^{-6} s^{-1} for $[MTBE]_0 = 1$ mM. These reaction rates are small enough to be ignored when compared with the effects of sonication. From Table 1, it is clear that the combination of O_3 and ultrasound increases k_0. The enhancement in k_0 is greater at lower $[MTBE]_0$. The enhancement factors (k_0(O_3–ultrasound)/k_0(ultrasound)) for 205 and 358 kHz are very similar at higher initial MTBE concentrations and increase slowly as $[MTBE]_0$ decreases. However, at lower concentrations (i.e., 0.01 mM), the enhancement factor for 358 kHz (5.4) is higher than it is at 205 kHz (3.9). The k_0 ratios at 358 and 205 kHz for the ultrasound system alone and the combined O_3–ultrasound system are also given in Table 1. For the ultrasound alone system, k_0 at 358 kHz was greater than at 205 kHz by a factor of 1.7–2.2. Similarly, in the case of the O_3–ultrasound system, the k_0 at 358 kHz was greater at lower $[MTBE]_0$.

The Role of Ozone in Sonochemistry. The combination of ozone and sonolysis was found to be significantly more effective in degrading MTBE than either ultrasound or O_3 alone (*14*). To illustrate the mechanism of ozone enhancement in the sonochemical process, the role of ozone in the sonolysis process was studied at the other target frequencies. In this study, the sonolysis rate of ozone was investigated as a function of frequency, power density, and $[MTBE]_0$. Aqueous ozone concentrations were determined by using continuous flow spectrophotometry at $\lambda = 260$ nm, where $\epsilon = 3300$ M^{-1} cm^{-1}.

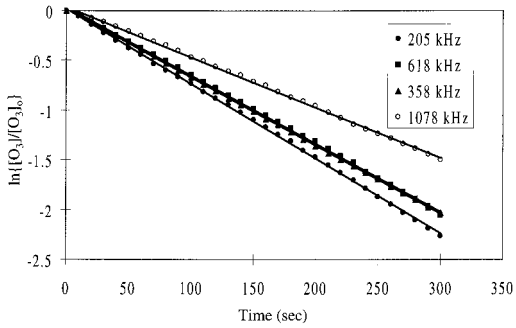

FIGURE 5. Effect of frequency on the first-order ozone degradation rate with power intensity = 100 W L^{-1}, $[O_3] = 0.14$–0.15 mM, $[HCO_3^-] = 1$ mM, and pH = 8.25.

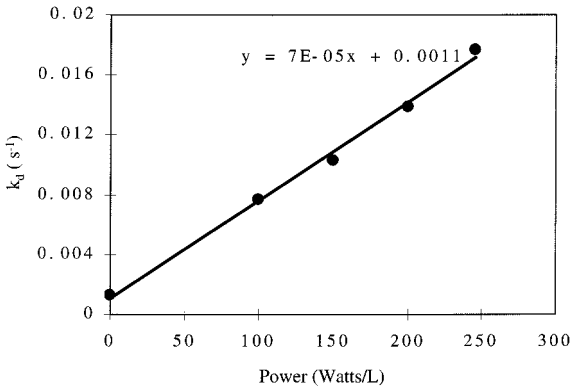

FIGURE 6. Effect of power density on the first-order ozone decay rate constant, k_d, for the sonolytic ozonolysis at 358 kHz: $[O_3] = 0.17$–0.18 mM; $[HCO_3^-] = 1$ mM; pH = 8.25.

In order to observe the relative effects of frequency on the ozone decomposition rate during sonication, initial aqueous ozone concentrations were adjusted to 0.13–0.15 mM before sonication and the aqueous ozone concentrations were monitored at 10 s intervals. Experiments were performed at a fixed power density of 100 W L^{-1} for all frequencies in a 1.0 mM bicarbonate [HCO_3^-] solution. As shown in Figure 5, the sonolytic degradation rate of ozone is found to be first order at all frequencies. Thus, the apparent rate equation for the sonolytic degradation of O_3 by sonolysis is given by eq 21, where k_d is the apparent first-order degradation rate constant. On the basis of the data, k_d is lowest at the highest ultrasonic frequency, 1078 kHz, while the measured rates at the other frequencies are nearly the same.

$$-d[O_3]/dt = k_d[O_3] \quad (21)$$

The relative effect of applied power density on the ozone decay rate was investigated at 358 kHz in 1.0 mM bicarbonate spiked distilled water. As shown in Figure 6, a linear dependence of the first-order rate constant for ozone with a variation of power density can be quantified as follows:

$$k_d = \gamma_0 + \gamma P \quad (22)$$

Where γ_0 is the ozone decay rate in the absence of ultrasound (0.0011 s^{-1}), i.e., the rate due to the base-catalyzed reaction $k_{O_3,OH^-}[OH^-]$, γ is the slope of the k_d vs P line (7.0×10^{-5}

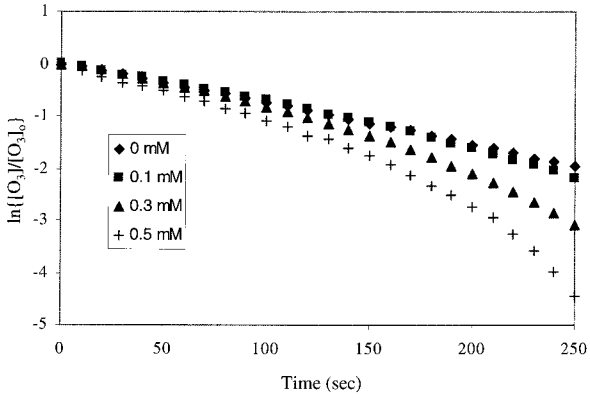

FIGURE 7. Effect of $[MTBE]_0$ on the first-order ozone degradation rate for the O_3−ultrasound process at 358 kHz: power density = 100 W L^{-1}; $[O_3]$ = 0.16−0.18 mM; $[HCO_3^-]$ = 1 mM; pH = 8.25.

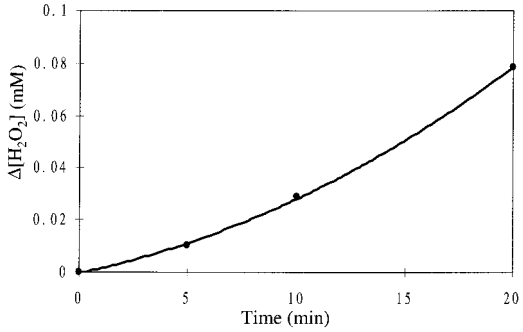

FIGURE 8. Net increased peroxide concentration, $\Delta[H_2O_2]$, versus time profile by the O_3−ultrasound process at 358 kHz: power density = 100 W L^{-1}, $[MTBE]_0$ = 0.5 mM; $[O_3]$ = 0.16 mM; $[HCO_3^-]$ = 1 mM; pH = 8.25.

L s^{-1} W^{-1}) and P is the power density in watts per liter. The overall decomposition rate, k_d, is the sum of the rate due to the base-catalyzed reaction pathway, the in situ thermal (pyrolysis) decomposition rate, and the ozone decay rate due to the conjugate base of H_2O_2 produced as a sonolysis intermediate.

$$H_2O_2 \leftrightarrow HO_2^- + H^+, \quad pK_a = 11.8 \tag{23}$$

Thus, k_d is given by

$$k_d = k_{O_3,OH^-}[OH^-] + k_{O_3,pyr} + 10^{pH-pK_a}k_{O_3,HO_2^-}[H_2O_2] \tag{24}$$

The effects of $[MTBE]_0$ on the ozone sonolytic decomposition rates are shown in Figure 7. In the absence of sonication, the ozone decay rates were not affected by the $[MTBE]_0$ due to the negligibly low rate of the direct reaction of ozone with MTBE at ambient temperature. However, the effect of $[MTBE]_0$ on the ozone decomposition rate is significant for sonolytic ozonolysis, as shown in Figure 7. In this case, the ozone decomposed at a faster rate with increasing $[MTBE]_0$. Furthermore, as $[MTBE]_0$ increases, the ozone decomposition rates deviate from a strict first-order relationship. This effect may be attributed to the direct reaction of MTBE with ozone at the cavitation bubble interface area or to the enhanced ozone decomposition rate due to the increased H_2O_2 production in the presence of MTBE (*14*). Thus, in the presence of MTBE, the sonolytic decomposition rate of ozone, $d[O_3]/dt$, is given by

$$-d[O_3]/dt = (k_d + k_{O_3,MTBE}[MTBE] + 10^{pH-pK_a}k_{O_3,HO_2^-}[H_2O_2])[O_3] \tag{25}$$

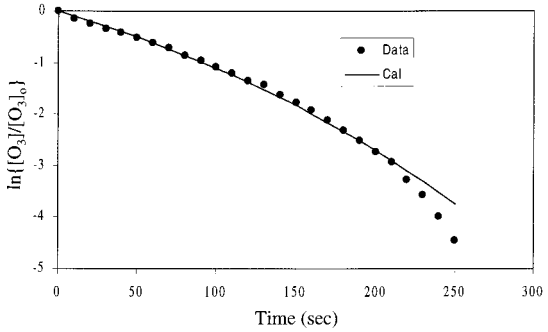

FIGURE 9. Comparison of the calculated and measured ozone degradation rate by the O_3−ultrasound process at 358 kHz: power density = 100 W L^{-1}; $[MTBE]_0$ = 0.5 mM; $[O_3]$ = 0.16 mM; $[HCO_3^-]$ = 1 mM; pH = 8.25.

where the first term represents the ozone decay rate in the absence of MTBE and the second and third terms are the net increased rates of ozone decay when MTBE is present.

Under these conditions, the sonolytic degradation of MTBE in the presence of O_3 is given by

$$[MTBE]_t = [MTBE]_0 e^{-k_0 t} \tag{26}$$

$\Delta[H_2O_2]$ is the net increase of $[H_2O_2]$ in the combined system in the presence of MTBE compared to the MTBE-free sonolysis. The $\Delta[H_2O_2]$ vs time profile obtained from measuring the $[H_2O_2]$ production rate at $[MTBE]_0$ = 0.5 mM relative to $[MTBE]_0$ = 0 mM is shown in Figure 8. The apparent increase in $d[H_2O_2]/dt$ can be attributed to the following reactions (*14*):

$$H_2O \xrightarrow{)))\Delta} H^\bullet + {}^\bullet OH \tag{27}$$

$$O_3 \xrightarrow{)))\Delta} O_2 + O^\bullet \tag{28}$$

$$(CH_3)_3COCH_3 + {}^\bullet OH \rightarrow (CH_3)_3COCH_2^\bullet + H_2O \tag{29}$$

$$(CH_3)_3COCH_2^\bullet + O_2 \rightarrow (CH_3)_3COCH_2O_2^\bullet \tag{30}$$

$$(CH_3)_3COCH_2O_2^\bullet + {}^\bullet OH \rightarrow (CH_3)_3COCHO + H_2O_2 \tag{31}$$

The $[H_2O_2]$ contributed from MTBE is a complicated process. We suppose the $\Delta[H_2O_2]$ vs time is a second-order polynomial equation as given by

$$\Delta[H_2O_2]_t = A_2t^2 + A_1t \tag{32}$$

The fitted result is shown in Figure 8 with $A_2 = 5.56 \times 10^{-8}$ and $A_1 = 2.0 \times 10^{-4}$. The influence to $[H_2O_2]$ from the first term is smaller than the second one at t < 100 min.

Substituting eqs 26 and 32 into eq 25 and rearranging in an integrated form yield

$$-\ln[O_3]/[O_3]_0 = k_d + (1 - e^{-k_0 t})k_{O_3,MTBE}[MTBE]_0/k_0 + 10^{pH-pK_a}k_{O_3,HO_2^-}(A_1t^2/2 + A_2t^3/3) \tag{33}$$

where k_{O_3,HO_2^-} is the second-order rate constant of O_3 and HO_2^- ($k_{O_3,HO_2^-} = 5.6 \times 10^6$ M^{-1} s^{-1}) (*21*). The pK_a for H_2O_2 = 11.8 and the pH = 8.25 in the 1.0 mM of $[HCO_3^-]$. The rate constant, $k_{O_3,MTBE}$, is estimated by fitting eq 33 to the experimental data. The fitted result is shown in Figure 9. In this case, $k_{O_3,MTBE}$ = 2.5 M^{-1} s^{-1}. The third term of eq 33 accounts for the deviation from pseudo-first-order kinetics. In addition, the apparent enhancement in $k_{O_3,MTBE}$ may be due to enhanced mass transfer between the bubble and liquid in the presence of ultrasound.

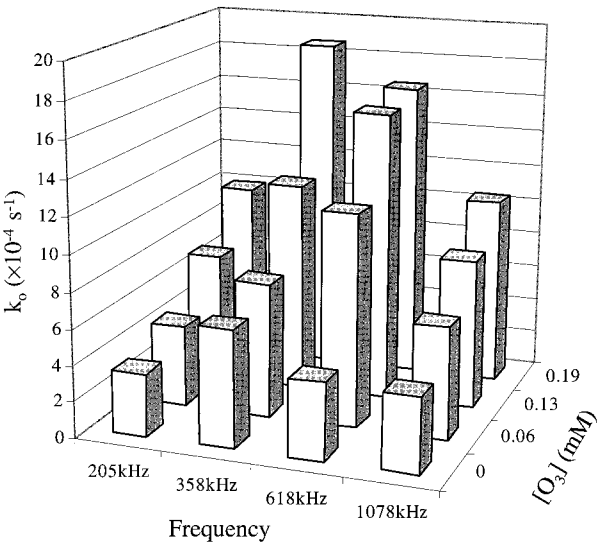

FIGURE 10. Effects of ozone and frequency on the pseudo-first-order rate constants for MTBE destruction: power density = 100 W L^{-1}; $[MTBE]_0$ = 0.05 mM.

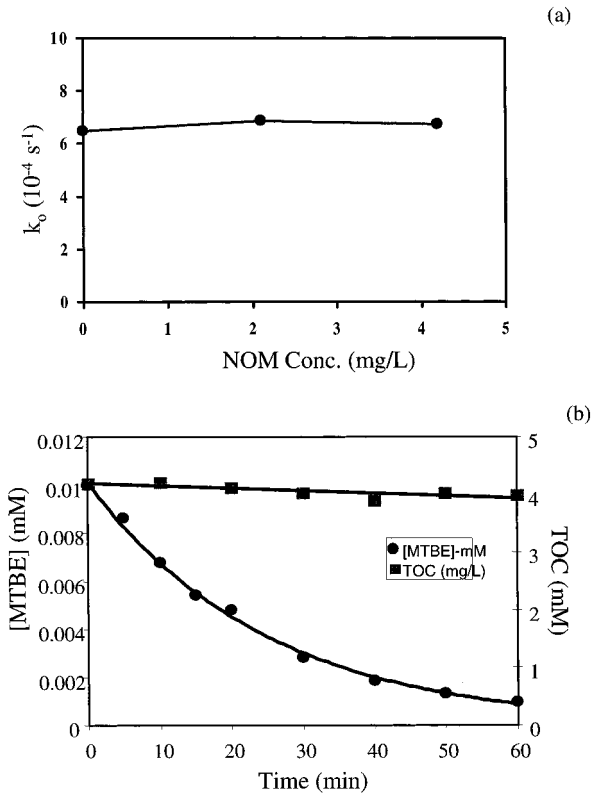

FIGURE 11. (a) Effect of NOM on the MTBE degradation rate by ultrasound at 358 kHz with a power density = 100 W L^{-1}. (b) Concentration of TOC as a function of time in the presence of humic acid.

Effects of Frequency and Ozone Concentration. The effects of frequency and ozone dose on the net MTBE degradation reaction rate were explored in order to obtain the overall optimal conditions. The pseudo-first-order rate constant, k_0, versus ozone concentration and frequency is shown in Figure 10. For each frequency, ozone doses were varied from 0 to 0.19 mM at $[MTBE]_0$ = 0.5 mM at a power density of 100 W L^{-1}. From the 3-D plot, it can be seen that ultrasonic frequencies of 358 and 618 kHz are the most effective for MTBE degradation. Without O_3, the rate constant of the sonolysis of MTBE has an optimal value at 358 kHz with a power density of 100 W/L. At the same power density, Petrier and Francony (*22*,*23*) reported that the sonolysis of phenol, a less volatile compound than CCl_4, has an optimal rate constant at 200 kHz compared to 20, 500, and 800 kHz.

The resonance radius of the bubble as described by Mason (*21*) is proportional to frequency^{-1} so the surface area-to-volume ratio is larger at higher frequencies. The rectified diffusion rate could also be enhanced at higher frequencies. For this reason the observed rate constant appears to be faster at 358 kHz than at 205 kHz.

Effect of Background Organics. Naturally occurring organic matter (NOM) and certain inorganic species in natural waters are potential competitive reactants for •OH. Therefore, these background components of natural waters may affect the observed oxidation rates. In order to test the potential impact of this type of competition for hydroxyl radical during sonication, MTBE was degraded in the absence and presence of NOM (i.e., made from Fluka AG) at concentrations of 2.1 and 4.2 mg/L. As shown in Figure 11a, the effect of NOM on the MTBE decomposition rate appears to be negligible. The concentration of TOC as a function of time in the presence of humic acid is shown in Figure 11b. This result confirms previous observations that the major reaction site for MTBE with •OH is in the vapor phase of the cavitation bubble and not in the bulk aqueous phase. For example, highly volatile compounds such as MTBE and CCl_4 are more rapidly decomposed during sonolysis than are semivolatile or nonvolatile compounds.

The results of this study demonstrate that the combination of ozonation and sonication can degrade MTBE more effectively at an ultrasonic frequency of 358 kHz compared to other available frequencies.

Acknowledgments

Financial support from the U. S. Department of Energy (Grant DOE 1 963472402) via the Argonne National Laboratory (Dr. Robert Peters) is gratefully acknowledged.

Literature Cited

(1) Suflita, J. M.; Mormile, M. R. *Environ. Sci. Technol.* **1993**, *27*, 976−978.
(2) Serpone, N.; Terzian, R.; Hidaka, H.; Pelizzetti, E. *J. Phys. Chem.* **1994**, *98*, 2634−2640.
(3) Kotronarou, A.; Mills, G.; Hoffmann, M. R. *Environ. Sci. Technol.* **1992**, *26*, 1460−1462.
(4) Kotronarou, A.; Mills, G.; Hoffmann, M. R. *J. Phys. Chem.* **1991**, *95*, 3630−3638.
(5) Hua, I.; Hoffmann, M. R. *Environ. Sci. Technol.* **1997**, *31*, 2237−2243.
(6) Hua, I.; Hoffmann, M. R. *Environ. Sci. Technol.* **1996**, *30*, 864−871.
(7) Hua, I.; Hochemer, R. H.; Hoffmann, M. R. *J. Phys. Chem.* **1995**, *99*, 2335−2342.
(8) Hua, I.; Hochemer, R. H.; Hoffmann, M. R. *Environ. Sci. Technol.* **1995**, *29*, 2790−2796.
(9) Mason, T. J.; Lorimer, J. P. *Sonochemistry: Theory, Application and Uses of Ultrasound in Chemistry*; John Wiley & Sons: New York, 1988.
(10) Flint, E. B.; Suslick, K. S. *Science* **1991**, *253*, 1397−1399.
(11) Hart, E. J.; Henglein, A. *J. Phys. Chem.* **1986**, *90*, 3061−3062.
(12) Olson, T. M.; Barbier, P. F. *Water Res.* **1994**, *28*, 1383−1391.
(13) Hart, E. J.; Henglein, A. *J. Phys. Chem.* **1985**, *89*, 4342−4347.
(14) Kang, J. W.; Hoffmann, M. R. *Environ. Sci. Technol.* **1997**, *32*, 3194−3199.
(15) Buxton, G. V.; Greenstock, C. L.; Helman, W. P.; Ross, A. B. *J. Phys. Chem. Ref. Data* **1988**, *17*, 513−886.
(16) Tsang, W.; Hampson, R. F. *J. Phys. Chem. Ref. Data* **1986**, *15*, 1087−1279.
(17) Zellner, R.; Ewig, F.; Paschke, R.; Wagner, G. *J. Phys. Chem.* **1988**, *92*, 4184−4190.
(18) Henglein, A.; Kormann, C. *Int. J. Radiat. Biol. Relat. Stud. Phys. Chem. Med.* **1985**, *48*, 251−258.

(19) Christensen, H.; Sehested, K.; Corfitzen, H. *J. Phys. Chem*. **1982**, *86*, 1588−1590.
(20) Hung, H.-M.; Hoffmann, M. R. *The Effect of Frequency, Hydrostatic Pressure, and Sonication Power on Sonochemical Reactions*. Manuscript in preparation.
(21) Staehelin, J.; Hoigne, J. *Environ. Sci. Technol.* **1982**, *16*, 676−681.
(22) Petrier, C.; Francony, A. *Water Sci. Technol.* **1997**, *35*, 175−180.
(23) Petrier, C.; Francony, A. *Ultrason. Sonochem*. **1997**, *4*, 295−300.

Received for review October 7, 1998. Revised manuscript received March 29, 1999. Accepted June 16, 1999.

ES9810383